Asian Journal of Chemistry; Vol. 38, No. 9 (2026), 2323-2331
ASIAN JOURNAL OF CHEMISTRY
https://doi.org/10.14233/ajchem.2026.36464

Caffeine-Mediated Combustion Synthesis of Nanocrystalline ZnO and NiO for Degradation of Efficient Methyl Orange

K. KAMALAVENI*, and A. ILAMPARITHI

Department of Chemistry, Gobi Arts and Science College, Gobichettipalayam-638453, India

*Corresponding author: E-mail: kamalavenikche@gmail.com

Received: 19 May 2026 *Accepted*: 27 July 2026 *Published online*: 5 September 2026 AJC-22460

Caffeine-mediated ZnO and NiO nanoparticles were prepared through an eco-friendly solution combustion route. The synthesis yielded porous, nanocrystalline powders with high chemical purity and appreciable photocatalytic performance. X-ray diffraction patterns assigned the ZnO phase to the hexagonal wurtzite structure and the NiO phase to the cubic bunsenite structure. The crystallite dimensions estimated from the Scherrer equation were 31.2 ± 2.8 nm for ZnO and 22.9 ± 1.9 nm for NiO. FT-IR spectra contained the characteristic metal–oxygen vibrational bands corresponding to Zn–O and Ni–O bonds, confirming the formation of the oxide phases. Scanning electron microscopy (SEM) revealed irregular, porous particles with a tendency toward agglomeration at the nanoscale. Energy-dispersive X-ray spectroscopy detected the expected elemental constituents and confirmed the high purity of the synthesized materials. The optical band-gap energies calculated from UV-DRS absorption data were 2.98 eV for ZnO and 3.10 eV for NiO. Photoluminescence measurements revealed blue emission features associated with oxygen vacancy related defects and other localized electronic states. ZnO exhibited comparatively weaker emission intensity, which is consistent with a lower extent of photogenerated electron-hole recombination. The photocatalytic properties were assessed through the degradation of methyl orange under UV irradiation. ZnO attained 83.2% dye degradation within 120 min, while NiO achieved 77.56% degradation after 150 min.

Keywords: Caffeine, Combustion synthesis, Zinc oxide, Nickel oxide, Methyl orange, Degradation, Photocatalysis.

INTRODUCTION

Textile, printing, paper, leather and pharmaceutical industries generate large quantities of dye-contaminated wastewater, posing risks to aquatic ecosystems and human health [1]. The synthetic dyes are of particular concern due to their chemical stability, toxicity and resistance to conventional biological treatment [2]. Methyl orange (MO), an aromatic azo dye, is widely used as a model pollutant in photocatalytic studies due to its stable molecular structure and resistance to degradation under natural conditions [3]. The development of effective methods for the removal of such pollutants is closely related to United Nations Sustainable Development Goal 6 (SDG 6), which promotes clean water, sanitation and improved wastewater treatment.

Semiconductor photocatalysis has attracted considerable interest for the treatment of persistent organic pollutants. Light irradiation with sufficient energy generates electron-hole pairs in semiconductor materials, which can participate in the formation of reactive oxygen species such as hydroxyl ($^{\bullet}OH$) and superoxide ($^{\bullet}O_2^-$) radicals. These reactive species can attack organic molecules and promote their degradation toward simpler products such as CO_2 and H_2O [4,5]. The photocatalytic response of a semiconductor is governed by several material properties, such as crystal structure, crystallite size, morphology, surface defects, optical band gap and electron-hole recombination.

ZnO and NiO are semiconductor metal oxides with distinct structural and electronic characteristics. ZnO is an n-type semiconductor known for its high exciton binding energy, chemical stability, low toxicity and photocatalytic activity [6]. NiO is a p-type semiconductor with useful electronic properties and has been investigated in catalysis, energy storage, sensing and environmental applications [7]. A comparative study of these two oxides prepared under similar conditions can provide useful information on the relationship between their structural and optical properties and photocatalytic performance.

Solution combustion synthesis is a simple and rapid method for preparing metal oxide nanomaterials. The method involves an exothermic redox reaction between a metal salt precursor and an organic fuel, with the heat generated during combustion promoting oxide formation [8]. The rapid release of gaseous products such as CO_2, H_2O and N_2 can favour the development of porous structures and restrict excessive grain growth, which is beneficial for obtaining nanosized oxide powders. The combustion fuel has an important role in controlling the reaction temperature, combustion behaviour, crystallinity and morphology of the resulting oxide. Urea, glycine, citric acid and hexamethylenetetramine (HMTA) are frequently used fuels in solution combustion synthesis [9].

Caffeine ($C_8H_{10}N_4O_2$) is a naturally occurring nitrogen-containing organic compound that can serve as an alternative combustion fuel [10]. Its functional groups can interact with metal ions, while its thermal decomposition during combustion contributes to heat and gaseous product formation. These characteristics make caffeine suitable for exploring a greener route for the preparation of metal oxide nanomaterials. The use of a naturally occurring compound as both a combustion fuel and complexing agent can reduce reliance on conventional synthetic reagents and is consistent with the principles of green chemistry and SDG 12 [11,12]. In the present work, ZnO and NiO nanoparticles were synthesized by an eco-friendly solution combustion method using zinc nitrate and nickel nitrate as precursors and caffeine as the combustion fuel. The structural, morphological, compositional and optical characteristics of the synthesized nanoparticles were examined using XRD, FTIR, SEM, EDS, UV-visible spectroscopy and photoluminescence measurements. Their photocatalytic performance was assessed through the degradation of methyl orange under UV irradiation. Particular attention was given to the crystal structure, crystallite size, optical band gap and defect-related photoluminescence characteristics of ZnO and NiO and their relationship with photocatalytic activity.

EXPERIMENTAL

Analytical grade solvents and chemicals zinc nitrate hexahydrate (≥ 99%), nickel(II) nitrate hexahydrate (≥ 98%) and caffeine ($C_8H_{10}N_4O_2$, m.w. 194.19 g mol^{-1}) were used as received and were not further purified. The photocatalytic experiments employed methyl orange as the model pollutant, with demineralized water used as the solvent throughout the study.

Caffeine-assisted solution combustion: The green solution combustion method using caffeine as fuel and complexing agent was adopted to prepare ZnO and NiO nanoparticles. For each of the typical synthesis, 0.1 mol of $Zn(NO_3)_2{\cdot}6H_2O$ (29.75 g) or $Ni(NO_3)_2{\cdot}6H_2O$ (29.08 g) was separately dissolved in 50 mL of demineralized water under magnetic stirring at laboratory temperature. A solution was prepared by adding 0.05 mol of caffeine (9.71 g) to each solution, with the fuel-to-oxidizer ratio as specified by the chemistry reactions and the resulting mixture stirred for 30 min until a clear homogeneous solution was formed. Excess water was removed from the solution by applying heat to a hot plate, so that it formed a viscous gel at 80-90 ºC. The gel self-sustained combustion reaction took place at temperatures around 250-300 ºC and a voluminous ash resulted in the release of various gases such as CO_2, H_2O and N_2. The as-combusted powders were then gently ground and calcined in air at 500 ºC for 3 h to increase the crystallinity and to remove the residual organic species. The idealized combustion reactions are given as:

$$2Zn(NO_3)_2{\cdot}6H_2O + C_8H_{10}N_4O_2 + 4.5O_2 \longrightarrow 2ZnO + 8CO_2 + 17H_2O + 6N_2\uparrow$$

$$2Ni(NO_3)_2{\cdot}6H_2O + C_8H_{10}N_4O_2 + 4.5O_2 \longrightarrow 2NiO + 8CO_2 + 17H_2O + 6N_2\uparrow$$

Characterization: An X-ray diffractometer (Bruker D8 advance, Cu*K*α radiation, λ = 1.5406 Å) measured the X-ray diffraction pattern from 20º to 80º 2θ. The crystallite size was calculated from major diffraction peaks using the Scherrer equation to obtain an average size. Surface functional groups and metal–oxygen vibrations were recorded with a Thermo Scientific Nicolet iS50 FTIR spectrometer in the range 4000-400 cm^{-1}. Surface morphology and elemental composition were studied with a Zeiss SEM and EDX. Optical absorption was measured from 200-800 nm with a JASCO V-570 and optical band gap energies were calculated using Kubelka-Munk and Tauc plot analyses. Photoluminescence spectra at room temperature were measured with a JASCO FP-8300 to examine defects and charge-carrier recombination behaviour.

Methyl orange photodegradation: The synthesized caffeine-mediated ZnO and NiO nanoparticles were tested for their photocatalytic activities by using the model organic pollutant methyl orange. A typical experiment involved dissolving 10 mg of dye, methyl orange, in deionized water to make the dye solution. Then 50 mg photocatalyst was added to 100 mL of the dye solution and stirred magnetically in dark for 30 min to reach the adsorption–desorption equilibrium. Then, the suspension was illuminated with a 120 W mercury UV lamp as a light source while being stirred continuously and suspended. Aliquots were removed from the reaction solution at certain periods, centrifuged to collect the catalyst particles and the remaining dye concentration was measured with a JASCO V-360 spectrometer based on the absorption peak of methyl orange at around 464 nm to 470 nm. The degradation efficiency was calculated using eqn. 1 [13]:

$$\text{Degradation } (\eta, \%) = \left(1 - \frac{C_t}{C_o}\right) \times 100 \quad (1)$$

where C_t is the dye concentration at varying time intervals, C_o is the initial concentration. The stability and reusability of synthesized caffeine-mediated ZnO and NiO nanoparticles were investigated by performing five consecutive cycles of photocatalytic degradation of methyl orange under the same experimental conditions. The photocatalyst was recovered by centrifugation after each cycle, washed with some deionized water and then ethanol to remove the adsorbed reaction intermediates and dried at 80 ºC for 2 h before being reused in the next degradation experiment. The degradation efficiency was determined after each cycle to evaluate the stability and reusability of the photocatalyst.

RESULTS AND DISCUSSION

XRD studies: The crystal structure and phase purity of the synthesized caffeine-mediated ZnO and NiO nanoparticles

using caffeine as a bio-derived fuel were investigated by X-ray diffraction (XRD) and the corresponding diffraction patterns are shown in Fig. 1. The ZnO sample exhibits sharp and intense reflections located at 2θ ≈ 31.7º, 34.3º, 36.3º, 47.7º, 56.8º, 62.5º, 66.3º, 67.7º and 69.3º, which can be indexed to the (100), (002), (101), (102), (110), (103), (200), (112) and (201) planes of the hexagonal wurtzite structure of ZnO (space group *P*63*mc*), consistent with standard JCPDS card No. 36-1451 [14]. As no additional diffraction peaks were observed, confirmed that the ZnO sample was free from detectable secondary phases. Similarly, the NiO sample displays characteristic diffraction peaks at 2θ ≈ 37.1º, 43.4º, 62.8º, 75.5º and 79.3º, corresponding to the (111), (200), (220), (311) and (222) crystal planes of cubic NiO (space group $Fm\bar{3}m$), in agreement with JCPDS card No. 47-1049 [15]. No diffraction peaks other than those assigned to NiO were detected, thereby confirmed the absence of detectable secondary phases in the sample.

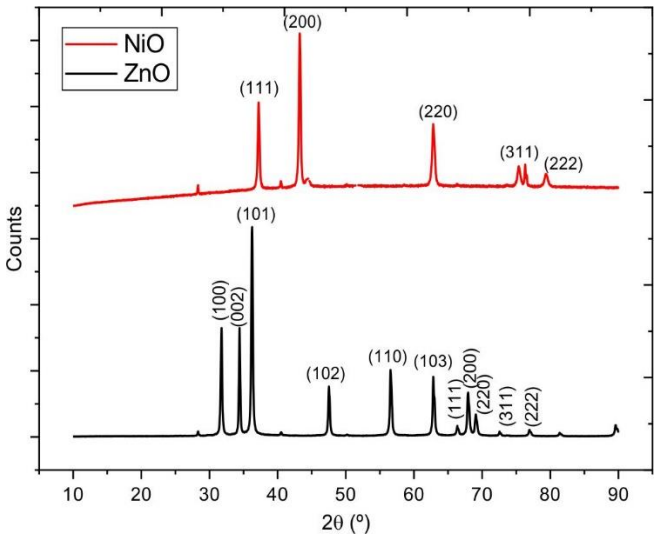

Fig. 1. XRD patterns of ZnO and NiO nanoparticles synthesized by caffeine assisted solution combustion

Both oxides exhibited sharp, intense diffraction peaks characteristic of well-crystallized materials. The good crystallinity can be linked to the high local temperatures generated during the combustion reaction. In this process, caffeine functioned as both the combustion fuel and complexing agent, while the metal nitrates provided the oxidizing component. The exothermic reaction is self-sustaining and when the precursor solution is heated, a huge volume of gaseous products (CO_2, H_2O, N_2) are produced which do not allow agglomeration of particles and hence generate highly porous nanostructured powders. All the significant diffraction peaks were used to estimate the crystallite size of the combustion synthesized ZnO and NiO nanoparticles using the Scherrer's equation [16].

$$D = \frac{K\lambda}{\beta \cos\theta} \quad (2)$$

where D is the crystallite size (nm), k is the shape factor (0.9), λ is the wavelength of Cu*K*α radiation (1.5406 Å), β is the full width at half maximum (FWHM) in radians and θ is the Bragg angle. Each diffraction peak was calculated to its respective size and then the average crystallite size was calculated as the mean of the sizes. The crystallite sizes calculated for ZnO and NiO were 31.2 ± 2.8 nm and 22.9 ± 1.9 nm, respectively, consistent with their nanocrystalline nature. The close similarity in crystallite sizes obtained from the different diffraction planes is associated with good crystallinity and high phase purity of the combustion-derived ZnO and NiO nanoparticles. The crystallite size values obtained from the different diffraction reflections were closely comparable, pointing to a uniform growth pattern within the crystallites. NiO had a smaller average crystallite size than ZnO, which may arise from differences in the growth behaviour during combustion. The sharp diffraction peaks and narrow peak widths are characteristic of highly crystalline ZnO and NiO nanoparticles with nanoscale crystallite dimensions.

FTIR studies: FTIR spectroscopy was used to examine the functional groups and metal–oxygen bonding in the combustion derived ZnO and NiO nanoparticles prepared using caffeine as a bio-derived fuel. The spectra were recorded over the range of 4000-400 cm^{-1} (Fig. 2). A weak, broad absorption band around 3500-3400 cm^{-1} was observed in both spectra, which can be assigned to O–H stretching from surface hydroxyl groups and adsorbed moisture [17]. The bands at 1650-1630 cm^{-1} are associated with the bending vibration of molecularly adsorbed water [18]. A weak feature in the 1450-1380 cm^{-1} region can be related to residual nitrate species and minor carbon-containing residues from the combustion process [19].

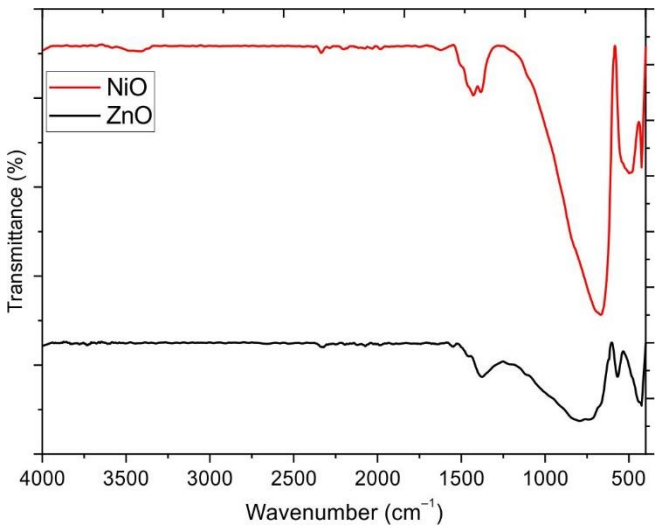

Fig. 2. FTIR spectra of ZnO and NiO nanoparticles showing characteristic metal–oxygen vibrations

The ZnO spectrum displayed a broad, intense absorption below 600 cm^{-1}, with the main band located at approximately 520-450 cm^{-1}, corresponding to Zn–O lattice vibrations of the wurtzite ZnO structure [18]. No appreciable bands were detected in the regions associated with C–H (3000-2800 cm^{-1}), C=O (1750-1650 cm^{-1}) and C–N (1350-1200 cm^{-1}) vibrations confirmed effective decomposition of the caffeine during combustion and subsequent heat treatment [20]. The NiO spectrum contained a strong absorption band in the 560-420 cm^{-1}, assigned to Ni–O lattice vibrations in cubic NiO [21]. The broad feature between 600 and 1100 cm^{-1} may arise from

surface hydroxyl species and metal–oxygen lattice vibrations. A weak band near 1450 cm^{-1} can be attributed to a small amount of surface carbonate formed through the adsorption of atmospheric CO_2. The absence of distinct organic-group vibrations is consistent with substantial decomposition of the caffeine fuel during combustion and conversion of the nickel precursor to NiO. The FTIR results establish the presence of Zn–O and Ni–O bonds in the respective samples, with only minor surface-adsorbed species. The hydroxyl- and carbonate-related bands are consistent with the interaction of nanostructured oxide surfaces with moisture and atmospheric CO_2.

UV-DRS spectral studies: The diffuse reflectance spectra of the combustion synthesized ZnO and NiO nanoparticles prepared using caffeine as green fuel in the wavelength range 200-800 nm was studied using UV-DRS spectroscopy. The ZnO nanoparticles show a strong absorption edge in the ultraviolet region at ~360-380 nm, which is characteristic of the transition of the electron from the valence band to the conduction band (direct electronic transition) [22]. The NiO nanoparticles show a wide absorption edge around 390-410 nm, corresponding to the charge transfer transition between the O 2*p* and Ni 3*d* orbitals [23] (Fig. 3). The wider absorption spectrum of NiO suggests the presence of defect states and intrinsic energy levels typical of nanocrystalline p-type semiconductors. The Kubelka-Munk function and Tauc plot methods were used to estimate the optical band gap energies. The reflectance data were converted using [24]:

$$F(R) = \frac{(1-R)^2}{2R} \quad (3)$$

where R is the diffuse reflectance. The absorption coefficient was then related to photon energy using the Tauc equation [25]:

$$(F(R)h\nu)^n = A(h\nu - E_g) \quad (4)$$

where F(R) is the Kubelka-Munk function, hν is the photon energy, A is a proportionality constant, E_g is the optical band gap energy, n = 2 for a direct allowed transition. Accordingly, plots of $(F(R)h\nu)^2$ *versus* hν were constructed and the linear portion was extrapolated to intersect the energy axis, where:

$$E_g = h\nu \text{ at } (F(R)h\nu)^2 = 0 \quad (5)$$

The calculated band gap energies were found to be 2.98 eV for ZnO and 3.10 eV for NiO as shown in Fig. 3b. The ZnO band gap was slightly lower than the reported value for bulk ZnO (3.2-3.3 eV), which may be related to nanoscale effects and defect states formed during caffeine-assisted combustion. This lower band-gap value can favour light absorption in the photocatalytic process. NiO exhibited a band gap of 3.10 eV, with its optical behaviour influenced by its p-type nature and defect states. The UV-visible absorption spectra and Tauc plots provide evidence of the optical characteristics of the combustion-derived ZnO and NiO nanoparticles. Their band-gap values and defect-related features make these materials suitable for investigation in photocatalytic applications.

SEM-EDX: The surface morphology and elemental composition of the caffeine-assisted combustion-derived ZnO and NiO nanoparticles were examined by SEM coupled with EDS. Both samples exhibited porous, agglomerated structures composed of predominantly spherical primary particles (Fig. 4) [26]. ZnO showed a loosely packed morphology, with fine nanoparticles connected to one another and occasional flower-like crystallite structures [27]. The pronounced porosity can be related to the rapid release of gaseous products such as CO_2, H_2O and N_2 during the combustion of the metal nitrates with caffeine. NiO consisted of irregular granular clusters with a

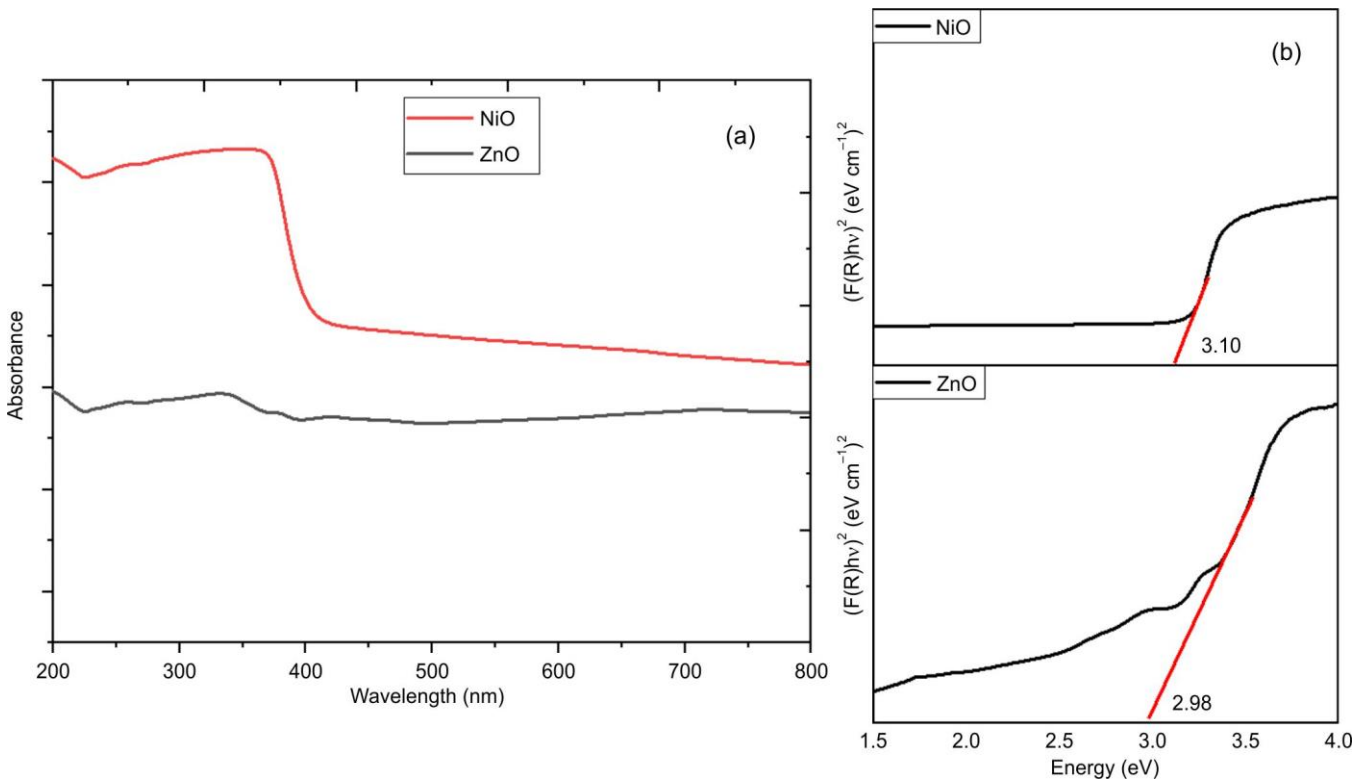

Fig. 3. (a) UV-Vis absorption spectra and (b) Tauc plots of ZnO and NiO nanoparticles

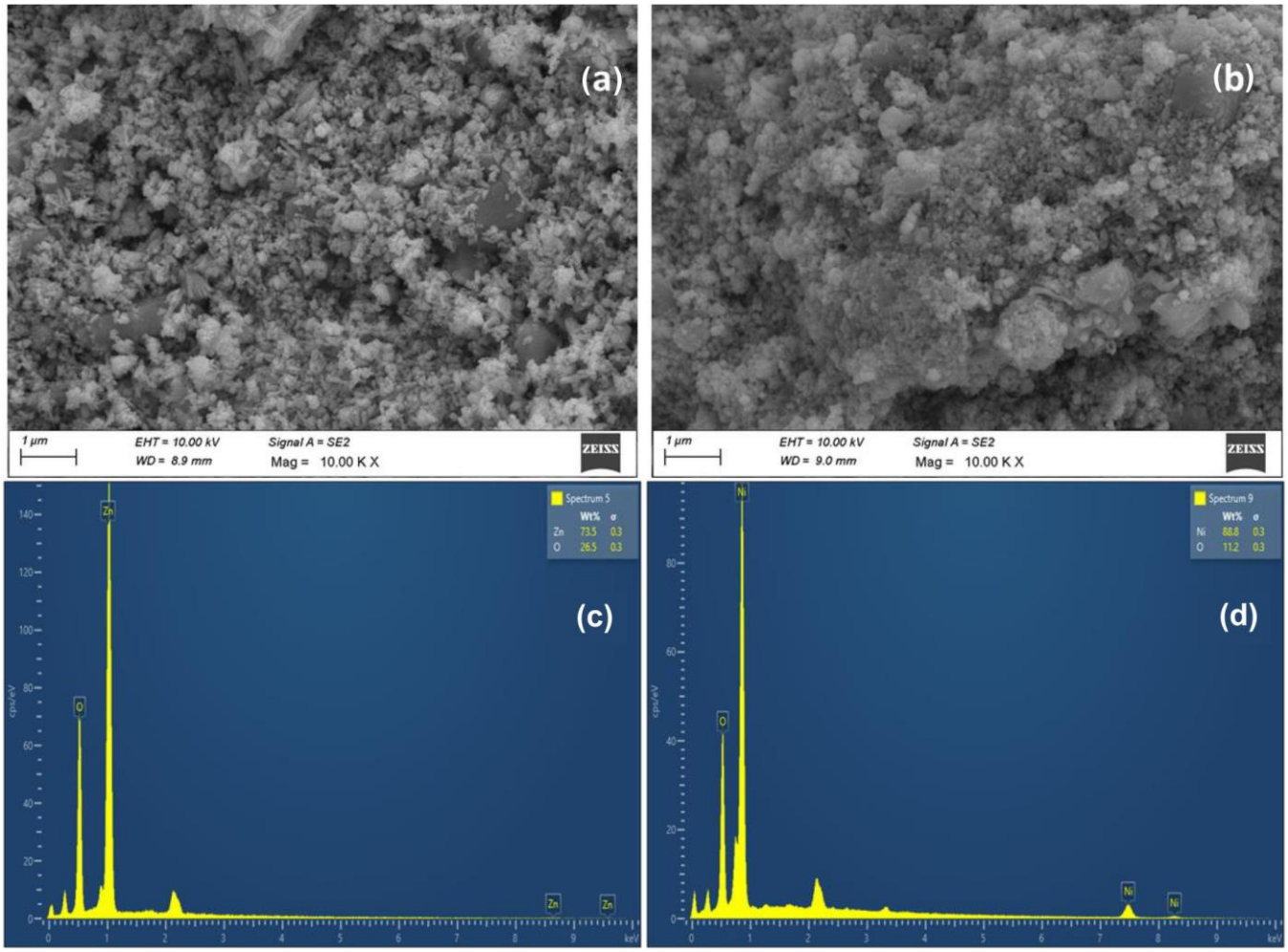

Fig. 4. SEM images and EDS spectra of ZnO (a,c) and NiO (b,d) nanoparticles

rough and highly porous surface. The nanosized primary particles were closely associated within larger secondary aggregates. Such a porous structure provides greater accessible surface area and can favour the transport of reactants and charge carriers during photocatalytic processes.

The EDS spectra contained only the elemental signals expected for the respective oxides. ZnO exhibited Zn Lα, Zn Kα, Zn Kβ and O Kα peaks, while the NiO spectrum contained Ni Lα (≈0.85 keV), Ni Kα (≈7.48 keV) and O Kα signals. Quantitative EDS analysis of NiO gave 88.8 wt.% Ni and 11.2 wt.% O. No distinct signals from foreign elements or unreacted precursor species were detected [28]. The small deviation from the theoretical composition can be associated with the lower detection sensitivity of EDS toward light elements and the presence of surface-adsorbed hydroxyl or carbonate species. The SEM and EDS results indicate that caffeine-assisted combustion yields porous, nanosized ZnO and NiO NPs with good chemical purity.

Photoluminescence: Photoluminescence (PL) measurements were carried out in the 320-530 nm range to examine the defect states and recombination behaviour of photogenerated charge carriers in the caffeine-assisted combustion-derived ZnO and NiO nanoparticles (Fig. 5). Both samples exhibited broad emission bands in the blue region, associated

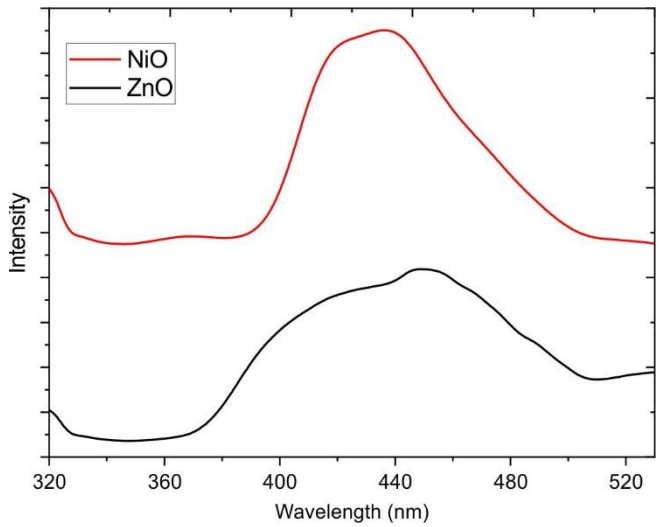

Fig. 5. Photoluminescence spectra of ZnO and NiO nanoparticles

with radiative transitions involving intrinsic and defect-related energy levels. The ZnO spectrum extended from approximately 390 to 500 nm, with a main emission peak near 450 nm. This emission can be related to oxygen vacancies, zinc interstitials and surface-related defect states [29]. The lower PL

intensity of ZnO points to reduced electron–hole recombination, which can favour the availability of photogenerated charge carriers for surface redox reactions during photocatalysis.

In case of NiO NPs, NiO exhibited a broader and more intense emission band between 400 and 520 nm, with the main peak located at approximately 440-445 nm. The blue emission may arise from charge-transfer transitions involving nickel vacancies, oxygen-related defects and Ni^{2+}/Ni^{3+} centers within the cubic NiO lattice [30]. The higher PL intensity of NiO is associated with a greater contribution from radiative recombination through defect-related states. These defect centers can influence light absorption and surface charge-transfer processes, while their presence is reflected in the broad emission profiles observed for both oxides. The broad PL bands can be associated with structural defects formed during the rapid combustion process. High local temperatures followed by rapid cooling can favour the formation of oxygen vacancies, cation vacancies, interstitial defects and other lattice imperfections. Such defects influence the optical response and charge-carrier dynamics of the nanoparticles and may affect their photocatalytic behaviour.

Photocatalytic degradation: The photocatalytic activity of the synthesized caffeine mediated ZnO and NiO nanoparticles was evaluated through the degradation of methyl orange (MO) under UV irradiation. The time-dependent UV-visible absorption spectra of MO in the presence of ZnO and NiO are shown in Fig. 6. The characteristic absorption band of MO at 464-470 nm gradually decreased with increasing irradiation time, exhibiting the progressive removal of the dye from the solution. The decrease in absorbance is associated with the breakdown of the azo (–N=N–) chromophore and subsequent degradation of the dye molecules [31].

ZnO NPs exhibited a faster degradation rate, with 83.2% removal of MO after 120 min of irradiation whereas NiO NPs showed a slower degradation process and reached 77.56% removal after 150 min. The dark and adsorption control experiments showed only limited changes in MO concentration in the absence of UV irradiation, while a marked decrease occurred in the presence of the photocatalysts under UV light. The higher activity of ZnO NPs can be related to its good crystallinity, lower PL intensity and porous morphology. The lower PL intensity is associated with reduced electron-hole recombination, while the porous structure provides accessible surface sites for dye adsorption and photocatalytic reactions. NiO NPs exhibited lower activity than ZnO NPs, although its defect states and optical response contributed to the degradation of MO during extended irradiation.

Under UV irradiation, electrons in the semiconductor are excited from the valence band to the conduction band, leaving holes in the valence band. The photogenerated electrons can react with dissolved O_2 to form superoxide radicals ($^{\bullet}O_2^-$), while the holes can react with surface-bound H_2O or hydroxyl groups to generate hydroxyl radicals ($^{\bullet}OH$). These reactive species attack the dye molecules and promote the breakdown of the azo chromophore, followed by further degradation of the resulting organic intermediates toward CO_2, H_2O and other less harmful products.

The two combustion-derived oxides showed appreciable photocatalytic activity toward MO degradation, with ZnO NPs exhibiting faster degradation and a higher removal efficiency than NiO NPs under the conditions used in this study. The results support the potential use of caffeine-assisted ZnO and NiO nanoparticles for photocatalytic treatment of dye-containing wastewater.

$$MO + h\nu \longrightarrow e^- + h^+$$

$$O_2 + e^- \longrightarrow {}^{\bullet}O_2^-$$

$$H_2O + h^+ \longrightarrow {}^{\bullet}OH + H^+$$

$$MO + {}^{\bullet}OH/{}^{\bullet}O_2^- \longrightarrow CO_2 + H_2O + \text{Mineralized products}$$

The correlation between concentration shifts and response time (min) is shown in Fig. 7. The rate constant for this degradation process is calculated using the following eqn. 6 and the kinetics are of pseudo-first order.

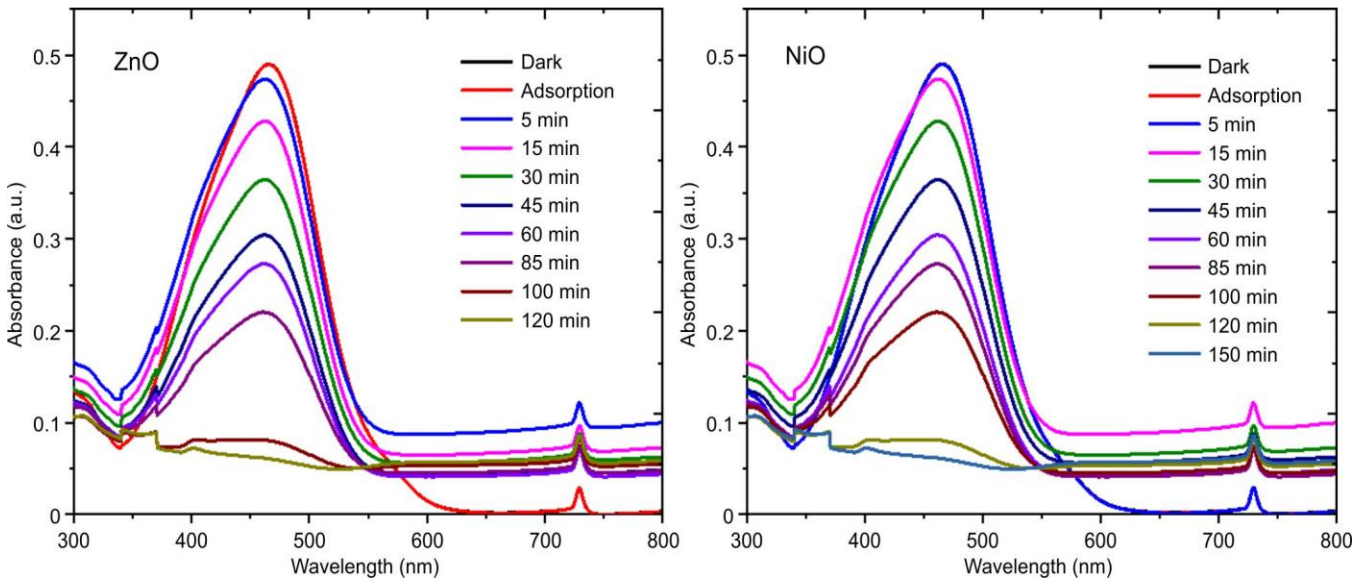

Fig. 6. UV-Vis spectra of methyl orange degradation using ZnO and NiO nanoparticles under UV irradiation

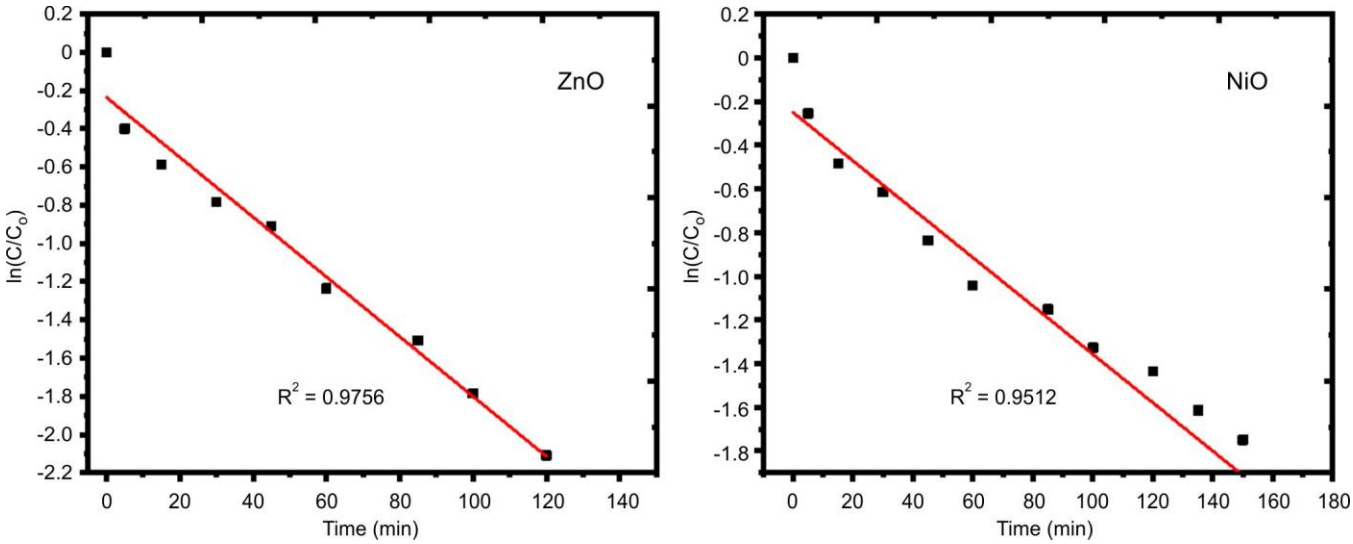

Fig. 7. Pseudo first-order kinetics for the photocatalytic degradation of MO by ZnO and NiO nanoparticles

$$\ln\left(\frac{C}{C_o}\right) = kt \quad (6)$$

A graph of ln (C/C_o) *vs.* reaction time from which the R^2 value and the rate constant (k) were computed to be 0.9756; 0.9512 and 0.0258 min^{-1}; 0.0213 min^{-1} for ZnO and NiO NPs, respectively.

The synthesized ZnO and NiO nanoparticles were investigated for their degradation efficiency through five successive cycles of photocatalytic degradation and the results are shown in Fig. 8. It can be observed that the degradation efficiency of the synthesized ZnO and NiO NPs has 95%, 91%, 85%, 79% and 71%, while 93%, 89%, 84%, 76% and 70%, respectively, for the first five cycles. The decrease in degradation efficiency is a gradual process, which is believed to be due to small losses of catalyst during the recovery process and possibly partial blocking of active sites by degradation intermediates strongly adsorbed on the surface. However, both caffeine mediated ZnO and NiO NPs retained nearly 75% of their initial photocatalytic efficiency after five consecutive cycles, with only a moderate decline in activity during reuse. The higher degradation efficiency maintained by ZnO NPs throughout the cycles is consistent with its stronger photocatalytic response toward MO dye.

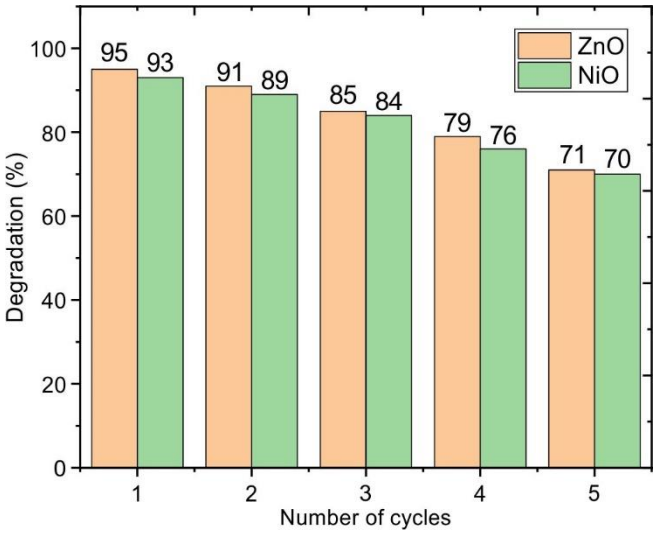

Fig. 8. Reusability of ZnO and NiO nanoparticles for the photocatalytic degradation of methyl orange over five consecutive cycles

A comparison of the present results with reported ZnO- and NiO-based photocatalysts is given in Table-1. The caffeine-assisted solution combustion route achieved MO degradation of 83.2% with ZnO and 77.56% with NiO under

TABLE-1
COMPARISON OF THE PHOTOCATALYTIC PERFORMANCE OF ZnO AND NiO NANOPARTICLES WITH PREVIOUSLY REPORTED STUDIES

Materials	Synthesis	Sources	Dyes	Time (min)	Degradation (%)	Ref.
ZnO and NiO	Sol-gel	Visible	MB	30	72.6-79.2	[32]
ZnO	Hydrothermal	UV	MB	80	50-62	[33]
NiO	Precipitation	UV	MB	180	96	[34]
ZnO	Sol-gel	Visible	RhB	180	90.25	[35]
NiO	Hydrothermal	Visible	MB	90	81	[36]
ZnO/NiO	Chemical	Visible	RhB	70	93.8	[37]
ZnO	Combustion	Visible	MB	60	84.29	[38]
NiO	Combustion	UV	Ferricyanide	30	84	[39]
ZnO	Combustion	UV	MO	120	83.2	This study
NiO	Combustion	UV	MO	150	77.56	This study

UV irradiation. Higher degradation values have been reported for some related photocatalysts, although the comparison is affected by differences in dye concentration, catalyst loading, irradiation source, reaction time and synthesis procedure. The results obtained in this study show that caffeine can be used as a bio-derived combustion fuel for the preparation of ZnO and NiO nanoparticles with appreciable photocatalytic activity. The method combines a short synthesis route with the use of a naturally occurring fuel and offers a practical approach for preparing oxide photocatalysts for dye-contaminated wastewater treatment.

Conclusion

The ZnO and NiO nanoparticles were synthesized using a simple, eco-friendly solution combustion method using caffeine as a green fuel and complexing agent. Caffeine replaces traditional fuels, aligning with green chemistry for nanomaterial production. X-ray diffraction confirmed the phase-pure hexagonal ZnO and cubic NiO structures, with average crystallite sizes of 31.2 ± 2.8 nm and 22.9 ± 1.9 nm, respectively. FTIR spectra exhibited the characteristic Zn–O and Ni–O vibrations of the respective oxides, while SEM images revealed porous, agglomerated nanoscale particles associated with rapid gas evolution during combustion. EDS analysis showed high chemical purity of the synthesized nanomaterials. The optical band gaps obtained from UV-DRS measurements were 2.98 eV for ZnO and 3.10 eV for NiO. PL spectra provided evidence of defect-related states that influence charge carrier recombination. Under UV irradiation, ZnO achieved 83.2% methyl orange degradation within 120 min, while NiO reached 77.56% after 150 min. The higher activity of ZnO can be related to its good crystallinity, lower electron–hole recombination and porous surface, while the defect-rich structure of NiO NPs contributed to its photocatalytic response. Caffeine-assisted solution combustion offers a simple, low-cost and environmentally considerate route for preparing ZnO and NiO nanoparticles. The photocatalytic performance and use of a bio-derived fuel make these materials promising for dye-contaminated wastewater treatment and support the broader goals of SDG 6 and SDG 12.

ACKNOWLEDGEMENTS

The authors are grateful to Gobi Arts and Science College, Gobi, for allowing the facility for this work.

CONFLICT OF INTEREST

The authors declare that there is no conflict of interests regarding the publication of this article.

DECLARATION OF AI-ASSISTED TECHNOLOGIES

During the preparation of this manuscript, the authors used an AI-assisted tool(s) to improve the language and no data, results or scientific conclusions were generated by AI. All analyses, interpretations and conclusions are the authors' own. The authors reviewed and edited the content and take full responsibility for the published work.

REFERENCES

1. A.P. Periyasamy, *Sustainability*, **16**, 495 (2024); https://doi.org/10.3390/su16020495
2. A. Negi, *Polymers*, **17**, 871 (2025); https://doi.org/10.3390/polym17070871
3. H. Alzain, V. Kalimugogo, K. Hussein and M. Karkadan, *Int. J. Res. Rev.*, **10**, 673 (2023); https://doi.org/10.52403/ijrr.20230682
4. M. Pavel, C. Anastasescu, R.-N. State, A. Vasile, F. Papa and I. Balint, *Catalysts*, **13**, 380 (2023); https://doi.org/10.3390/catal13020380
5. J. Zhang, G. Zhang, H. Lan, M. Sun, H. Liu and J. Qu, *Environ. Sci. Technol.*, **57**, 12117 (2023); https://doi.org/10.1021/acs.est.3c03406
6. S. Kumar, V. Kumar, C.S. Pathak, A. Mishra, M.K. Bansal and R.S. Baghel, *Results Mater.*, **30**, 100929 (2026); https://doi.org/10.1016/j.rinma.2026.100929.
7. M. Sultan, N. Ali, M. Naseem, S. Ihsan, M. Islam, A. Kareem, S. Khan, B.M. Khan, F. Khan, F. Ali, A. Khan, R.A. Al Balushi and M.M. Al-Hinaai, *Water Air Soil Pollut.*, **237**, 611 (2026); https://doi.org/10.1007/s11270-026-09274-x
8. A.A. Bayode, O.T. Ore, E.A. Nnamani, B. Sotunde, D.T. Koko, E.I. Unuabonah, B. Helmreich and M.O. Omorogie, *ACS Omega*, **9**, 19770 (2024); https://doi.org/10.1021/acsomega.4c01487
9. S. Padayatchee, H. Ibrahim, H.B. Friedrich, E.J. Olivier and P. Ntola, *Fluids*, **10**, 82 (2025); https://doi.org/10.3390/fluids10040082
10. A.A. Abu-Hashem, O. Hakami, M. El-Shazly, H.A.S. El-Nashar and M.N.M. Yousif, *Chem. Biodivers.*, **21**, e202400050 (2024); https://doi.org/10.1002/cbdv.202400050
11. M.M. Khairul Akter, U.N. Haq, M.M. Islam and M.A. Uddin, *Clean. Environ. Syst.*, **4**, 100070 (2022); https://doi.org/10.1016/j.cesys.2022.100070
12. S. Ying, Z. Guan, P. C. Ofoegbu, P. Clubb, C. Rico, F. He and J. Hong, *Environ. Technol. Innov.*, **26**, 102336 (2022); https://doi.org/10.1016/j.eti.2022.102336
13. Z. Lu, L. Guo, F. Bi, S. Ma, Q. Shen, R. Qiao and X. Zhang, *Sep. Purif. Technol.*, **354**, 129443 (2025); https://doi.org/10.1016/j.seppur.2024.129443
14. S. Sourav, S. Alam and H. Das, *Transition Met. Chem.*, **50**, 1 (2025); https://doi.org/10.1007/s11243-024-00600-y
15. M. Pushpa, Y. Patil, N.R.M. Banu and B. Pushpa, *J. Electrochem. Soc.*, **173**, 097501 (2026); https://doi.org/10.1149/1945-7111/ae62ae
16. N.N. Ahamed, J. Pattar, M.A. Kumar, N. Basavaraju and N. Raghavendra, *RSC Adv.*, **14**, 17664 (2024); https://doi.org/10.1039/D4RA01706D
17. S. Pasieczna-Patkowska, M. Cichy and J. Flieger, *Molecules*, **30**, 684 (2025); https://doi.org/10.3390/molecules30030684
18. M.O. Yusuf, *Appl. Sci.*, **13**, 3353 (2023); https://doi.org/10.3390/app13053353
19. Y. Bouramdane, M. Haddad, A. Mazar, S. Aît Lyazidi, H. Oudghiri Hassani and A. Boukir, *Polymers*, **16**, 3334 (2024); https://doi.org/10.3390/polym16233334
20. L. Yang and Y. Yuan, *Sci. Rep.*, **15**, 18676 (2025); https://doi.org/10.1038/s41598-025-03769-z
21. G. Rathika, R. Jagadeeswari, T. Sathiyapriya and P. Selvakumar, *Kuwait J. Sci.*, **51**, 100200 (2024); https://doi.org/10.1016/j.kjs.2024.100200
22. R. Gopalakrishnan and M. Ashokkumar, *J. Mater. Sci. Mater. Electron.*, **35**, 1614 (2024); https://doi.org/10.1007/s10854-024-13395-6
23. V.N. Hegde, *Mater. Chem. Phys.*, **333**, 130319 (2025); https://doi.org/10.1016/j.matchemphys.2024.130319
24. P.R. Jubu, O.S. Obaseki, D.I. Ajayi, E. Danladi, K.M. Chahrour, A. Muhammad, S. Landi Jr., T. Igbawua, H.F. Chahul and F.K. Yam, *J. Opt.*, **53**, 5054 (2024); https://doi.org/10.1007/s12596-024-01741-0

25. P.R. Jubu, O. Adedokun, C. Mbakaan, A. Nathan-Abutu, E. Danladi, J.N. Tsaviv, P.I. Kyesmen, B.J. Akeredolu, A.T. Adepoju, F. Aungwa, Y. Yusof, O.S. Obaseki, Y.S. Elzawiei and M.Z. Pakhuruddin, *J. Mater. Sci. Mater. Electron.*, **36**, 961 (2025); https://doi.org/10.1007/s10854-025-15037-x
26. M. Ahmaruzzaman, *Nanotechnol. Environ. Eng.*, **8**, 219 (2023); https://doi.org/10.1007/s41204-022-00284-8
27. Z.U. Abideen, Ph.D. Thesis, Flame Synthesized Nanoparticles and Miniaturized Opto-Electronic Devices for Advanced Gas Sensing, The Australian National Universitym Canberra, Australia (2024).
28. Q. An, J. You, T. Liu and J. Zhang, *Chem. Commun.*, **61**, 17559 (2025); https://doi.org/10.1039/d5cc04184h
29. Z. Yang, J. Mu, Z. Wang, S. Yu, X. Li, S. Du, Z. Yu, W. Sun and L. Zhao, *J. Alloys Compd.*, **1032**, 180878 (2025); https://doi.org/10.1016/j.jallcom.2025.180878
30. A.E. Alprol, A. Bakr, S.I. Al-Saeedi, E. El-Haroun and M. Ashour, *Front. Mar. Sci.*, **12**, 1624235 (2025); https://doi.org/10.3389/fmars.2025.1624235
31. L. Yadeta Gemachu and A. Lealem Birhanu, *Green Chem. Lett. Rev.*, **17**, 2293841 (2024); https://doi.org/10.1080/17518253.2023.2293841
32. K. Sahu and A.K. Kar, *Mater. Sci. Semicond. Process.*, **104**, 104648 (2019); https://doi.org/10.1016/j.mssp.2019.104648
33. H.S. Sumantha, S. Rajagopal, G. Nagaraju, M. Shashank and B.L. Suresha, *Chem. Phys. Lett.*, **779**, 138837 (2021); https://doi.org/10.1016/j.cplett.2021.138837
34. G.A. Gbair and H.A. Alshamsi, *Biomass Conv. Bioref.*, **14**, 28117 (2024); https://doi.org/10.1007/s13399-022-03408-x
35. E. Arulkumar and S. Thanikaikarasan, *Optik*, **302**, 171685 (2024); https://doi.org/10.1016/j.ijleo.2024.171685
36. S. Jolaei, M. Mirzaei, A. Hassanpour, H. Safardoust and A. Khani, *J. Nanostructures*, **12**, 761 (2022); https://doi.org/10.22052/JNS.2022.03.029
37. F. Rahman, M.A. Majed Patwary, M.A. Bakar Siddique, M.S. Bashar, M.A. Haque, B. Akter, R. Rashid, M.A. Haque and A.K.M. Royhan Uddin, *R. Soc. Open Sci.*, **9**, 220858 (2022); https://doi.org/10.1098/rsos.220858
38. A.K.H. Bashir, L.C. Razanamahandry, A.C. Nwanya, K. Kaviyarasu, W. Saban, H.E.A. Mohamed, S.K.O. Ntwampe, F.I. Ezema and M. Maaza, *J. Phys. Chem. Solids*, **134**, 133 (2019); https://doi.org/10.1016/j.jpcs.2019.05.048